Hindawi
Shock and Vibration
Volume 2023, Article ID 6225923, 15 pages
https://doi.org/10.1155/2023/6225923

Research Article

Mine Microseismic Signal Denoising Based on a Deep Convolutional Autoencoder

Ting Hu,[1,2] **Bin Xu**,[2] **Yongfa Wang**,[2] **Jiayi Zhu**,[2] **Jiang Zhou**,[1] **and Zhongyi Wan**[1]

[1]*Southwest Jiaotong University Hope College, Chengdu 610400, China*
[2]*Chengdu University of Technology, Geomathematics Key Laboratory of Sichuan Province, Chengdu 610059, China*

Correspondence should be addressed to Bin Xu; xubin20080108@163.com

Received 23 March 2023; Revised 19 July 2023; Accepted 3 August 2023; Published 30 August 2023

Academic Editor: Xian-Bo Wang

Mine microseismic signal denoising is a basic and crucial link in microseismic data processing, which influences the accuracy and reliability of the monitoring system, and is of great significance with regard to safety during mining. Therefore, this study introduces a deep learning method to improve the mapping function and sparsity of signals in the time-frequency domain and constructs a denoising framework based on a deep convolutional autoencoder to address the denoising problem of mine microseismic signals. First, all noisy microseismic signals are normalized to ensure the nonlinear expression ability of the constructed denoising framework. Then, the normalized signals are transformed into the time-frequency domain using the short-time Fourier transform (STFT), and the real and imaginary parts of time-frequency coefficients serve as the input of the deep convolutional autoencoder to output the masks of the effective and noise signals. Next, these masks are applied to the time-frequency coefficients of the noisy microseismic signals, and the time-frequency coefficients of the potentially effective and noise signals are estimated. Finally, inverse STFT is used to transform these time-frequency coefficients to the time domain to obtain the final denoised effective and noise signals. The constructed framework automatically learns rich features from synthetic data to separate the effective and noise signals, thereby achieving the purpose of fast and automatic denoising. The experimental results show that compared with the wavelet threshold and ensemble empirical mode decomposition, the denoising framework considerably improves the signal-to-noise ratio of mine microseismic signals with less waveform distortion. Moreover, it can achieve a better denoising effect efficiently even in the case of a low SNR, which has obvious advantages. The constructed denoising framework is suitable for microseismic monitoring signals of various mine dynamic disasters and provides strong technical support for intelligent monitoring and early warning concerning production risks in mines.

1. Introduction

With the rapid development of China's economy, the demand for various mineral resources has sharply increased. Therefore, it is imperative to expand the scale of mining and strengthen the exploration and exploitation of deep resources [1]. However, the security issues caused by complex, difficult, and deep mining have become increasingly prominent with the continuation of mining. Serious mine dynamic disasters and hidden dangers, such as roof fall, collapse, and rock burst, cause huge losses to people and their properties [2, 3]. Thus, continuously monitoring the rupture of rock masses, quantitatively evaluating the stability of underground surrounding rocks, and accurately predicting mine dynamic disasters have become crucial to mine safety [4]. Previous studies showed that microseismic monitoring is an effective technology for mine dynamic disaster monitoring and early warning [5, 6]. The main task in microseismic monitoring is to timely delineate dangerous areas by locating hypocenters, evaluating the stability of rocks, and predicting possible geological disasters [7]. Owing to the low signal-to-noise ratio (SNR) of microseismic signals, they must first be denoised to ensure the accuracy of first arrival picking and hypocenter location [8, 9].

Denoising is a classic problem in geophysics. Mine microseismic signals usually have nonlinear and nonstationary characteristics. Notably, traditional denoising

methods, such as Fourier transform [10], can suppress noise to a certain extent, but they are more suitable for dealing with stationary periodic signals. When processing nonstationary signals with spikes or sudden changes, such as microseismic signals, their denoising effect is not very satisfactory. For the denoising of nonlinear signals, researchers have proposed several methods, such as wavelet transform (WT) [11, 12], S transform [13], curvelet transform [14], dreamlet transform [15], contourlet transform [16], shearlet transform [17], and empirical mode decomposition (EMD) [18, 19]. These methods can improve the quality of microseismic signals; however, they have certain limitations in terms of their validity and practicality. In practical application, they generally require more manual participation, such as the basis function selection of WT and the intrinsic mode function (IMF) selection of EMD, considerably limiting their application scope [20, 21]. Furthermore, the denoising effect of these methods is not satisfactory under a low-SNR condition. After denoising, the effective signals are distorted, destroying the original amplitude characteristics of microseismic signals and reducing the fidelity of effective signals [22, 23]. Therefore, their denoising performance needs further improvement.

In all these methods, microseismic signals are first transformed from the time domain to the time-frequency domain using a time-frequency analysis method. Then, the time-frequency coefficients are modified (usually thresholded) to attenuate noise-related coefficients, and the values of the effective signal coefficients are estimated. Finally, the modified coefficients are inverse-transformed to the time domain to reconstruct the denoised signals [24, 25]. They are referred to as time-frequency domain denoising methods, which basically involve improving the sparsity of signals by transforming microseismic data to other spatial domains, wherein the signals can be represented by a set of sparse features, making it easier to separate the effective and noise signals [26, 27]. Time-frequency domain denoising methods are the main focus of current research on microseismic signal denoising. On the basis of considering the time-frequency representation of multiple traces as a 3-D tensor, Iqbal et al. [28] introduced an approach for detecting and denoising microseismic events using tensor decomposition, where the higher order and tensor singular value decomposition were used for detecting and denoising, respectively. To obtain a sparse time-frequency representation and have a higher energy concentration, Zhang et al. [29] proposed a denoising framework based on the cumulative distribution function thresholding in the wavelet domain using synchrosqueezed continuous wavelet transform (SS-CWT). To suppress isolated noise on the time-frequency plane using SS-CWT with hard thresholding, Zeng et al. [30] introduced an image processing approach called pixel connectivity thresholding to further improve the SNR of microseismic signals. More studies on time-frequency domain denoising of microseismic signals can be seen in the literature [12, 23, 31–33]. Generally, these methods can be used to improve the denoising effect in two ways: use a more flexible and powerful mapping function or use a more efficient sparse representation of the data [34–36]. However, how to map microseismic data into an optimal denoising space and choose an appropriate threshold function to separate the effective and noise signals is a great challenge [37].

Recently, with the development of deep learning technology, deep neural networks have been gradually applied to signal denoising. For the denoising of 1-D seismic signals, Iqbal [38] proposed a denoising method based on an intelligent deep convolutional neural network, which learns sparse representation of the data simultaneously in the time-frequency domain and adaptively captures seismic signals corrupted with noise. Othman et al. [39] proposed a fully automated event detection and denoising method for seismic data, where a residual neural network and an IIR Wiener filter were used to detect seismic events and denoise the seismic data, respectively. These networks can improve the denoising effect by using convolution to extract the features of signals and training to obtain their better sparse representations [40–42]. Therefore, a deep learning method is primarily used in this study to improve the mapping function and sparsity of signals to construct a novel time-frequency domain denoising framework, namely, a microseismic signal denoising method based on a deep convolutional autoencoder. This method can learn the sparse representations of input signals from the training set and generate two separate masks for each noisy microseismic signal according to these representations; the generated masks are then used to extract the effective and noise signals, thereby achieving the purpose of mine microseismic signal denoising. The main contributions of this study are outlined as follows:

(1) A fully automated denoising framework based on a deep convolutional autoencoder is constructed for mine microseismic signals.

(2) Despite only being trained on synthetic data, the denoising framework can be generalized to practical denoising tasks, and test results on a real dataset show better performance, denoising effect and computational efficiency, in comparison with two common denoising methods.

(3) Because it does not require any prior knowledge or preprocessing, the constructed denoising framework is suitable for microseismic monitoring signals of various mine dynamic disasters.

2. Methodology

In the time-frequency domain, each noisy microseismic signal $\mathbf{Y}(t, f)$ can be expressed as the superposition of an effective microseismic signal $\mathbf{S}(t, f)$ and a noise signal $\mathbf{N}(t, f)$ (a collective term for various noises or non-microseismic signals):

$$\mathbf{Y}(t, f) = \mathbf{S}(t, f) + \mathbf{N}(t, f). \tag{1}$$

The objective of denoising is to estimate the potential effective microseismic signal $\widehat{\mathbf{S}}(t, f)$ from the polluted signal under the condition of minimizing the error between the estimated and real signals [37], which is as follows:

$$\begin{aligned}\text{error} &= E\|\widehat{\mathbf{S}}(t,f) - \mathbf{S}(t,f)\|_2^2 \\ &= E\left\|\text{TFT}^{-1}\{\mathbf{M}(t,f)\mathbf{Y}(t,f)\} - \mathbf{S}(t,f)\right\|_2^2,\end{aligned} \tag{2}$$

where $\|\cdot\|_2$ represents the L2 norm, TFT^{-1} indicates inverse time-frequency transform, and $\mathbf{M}(t,f)$ represents the mapping function, which maps the noisy microseismic signal $\mathbf{Y}(t,f)$ to the time-frequency representation of the potential effective signal. The results of the study showed that this mapping can be obtained by using a simple threshold in a sparse representation, and its magnitude can be estimated based on the noise level [43].

2.1. Autoencoder. An autoencoder is an unsupervised feature extraction and data dimensionality reduction method [44]. It is a symmetric network consisting of an encoder, encoding, and decoder. The schematic of its network structure is shown in Figure 1.

Starting from the leftmost input layer, the input sample $\mathbf{X}$ is processed layer by layer through the hidden middle layers and finally reaches the output layer. The output $\widehat{\mathbf{X}}$ of the decoder can be considered as a prediction value of the input $\mathbf{X}$. The encoding and decoding processes can be expressed as formulas (3) and (4), respectively.

$$\mathbf{H} = g(\mathbf{W}_1\mathbf{X} + \mathbf{b}_1), \tag{3}$$

$$\widehat{\mathbf{X}} = g(\mathbf{W}_2\mathbf{H} + \mathbf{b}_2), \tag{4}$$

where $\mathbf{W}_1$ and $\mathbf{b}_1$ are the power matrix and bias between the input and encoding layers, respectively; $\mathbf{W}_2$ and $\mathbf{b}_2$ are the power matrix and bias between the encoding and output layers, respectively; $\mathbf{H}$ is the hidden variable; and $g(\cdot)$ is the activation function. The objective of network training is to minimize the loss function $J(\mathbf{W},\mathbf{b})$, namely,

$$\arg\min_{\mathbf{W},\mathbf{b}} J(\mathbf{W},\mathbf{b}), \tag{5}$$

where $\mathbf{W} = [\mathbf{W}_1\ \mathbf{W}_2]$ and $\mathbf{b} = [\mathbf{b}_1\ \mathbf{b}_2]$. In an autoencoder, since the number of nodes in the input and output layers is equal, it attempts to approximate an identity function through the encoding and decoding operations (so that the output value corresponds to the input value) to determine the hidden association structure in original data.

2.2. Convolutional Autoencoder. In a convolutional neural network, different features can be extracted from different convolutional layers [45], and both local and global features are beneficial to obtain clean effective microseismic signals. Therefore, in order to introduce a convolutional neural network into the denoising of microseismic signals, this study used the neural network to learn the sparse representations of the signals, generated an optimal mapping function for each signal according to the effective and noise signals in training samples, and defined the mapping functions as two separate masks, $\mathbf{M}_S(t,f)$ and $\mathbf{M}_N(t,f)$ [46], which represent the effective and noise signals, respectively:

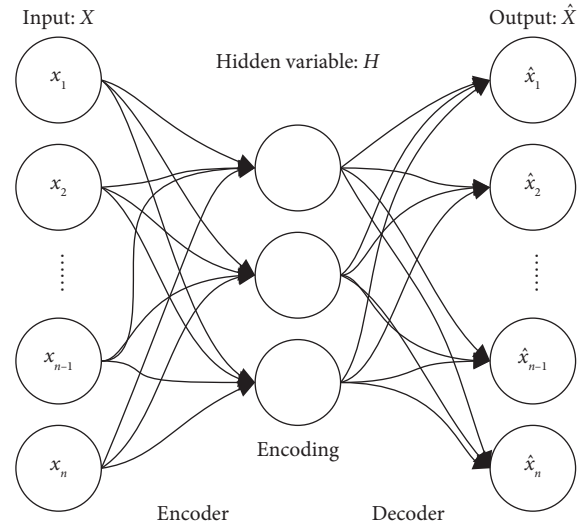

Figure 1: The network structure of an autoencoder.

$$\begin{cases}\mathbf{M}_S(t,f) = \dfrac{1}{1+|\mathbf{N}(t,f)|/|\mathbf{S}(t,f)|}, \\ \mathbf{M}_N(t,f) = \dfrac{|\mathbf{N}(t,f)|/|\mathbf{S}(t,f)|}{1+|\mathbf{N}(t,f)|/|\mathbf{S}(t,f)|}.\end{cases} \tag{6}$$

The size of each mask is the same as that of the input time-frequency microseismic signal $\mathbf{Y}(t,f)$, with the value being between 0 and 1, which indicates the proportion of corresponding signals, effective microseismic signal or noise signal, in a noisy microseismic signal.

The network structure of the deep convolutional autoencoder designed in this study according to the characteristics of the autoencoder and convolutional neural network is shown in Figure 2.

In the deep convolutional autoencoder network (Figure 2), the input of the first layer comprises the real and imaginary parts of the time-frequency representations for microseismic signals. The output comprises two masks, $\mathbf{M}_S(t,f)$ and $\mathbf{M}_N(t,f)$, respectively, of the effective and noise signals. The blue rectangles represent the inner layers of the network. In the first half of the network, the input time-frequency coefficients are first downsampled using multiple 3×3 convolutional layers with a stride of 2×2 and then processed using the activation layer of the rectified linear unit (ReLU) function after each convolutional layer. These convolutional layers act as feature extractors, compressing the feature maps and quickening the learning of the sparse representation of the input data to the bottleneck layer. In the second half of the network, the deconvolution layer upsamples to generate a high-dimensional nonlinear mapping of the sparse representations to the effective and noise signal masks, and the softmax function is used in the last layer to predict the difference between the effective and noise signal masks. These masks are considered the targets in optimizing the convolutional autoencoder network during training. Through training, the network learns how to construct a sparse representation of the data as well as how

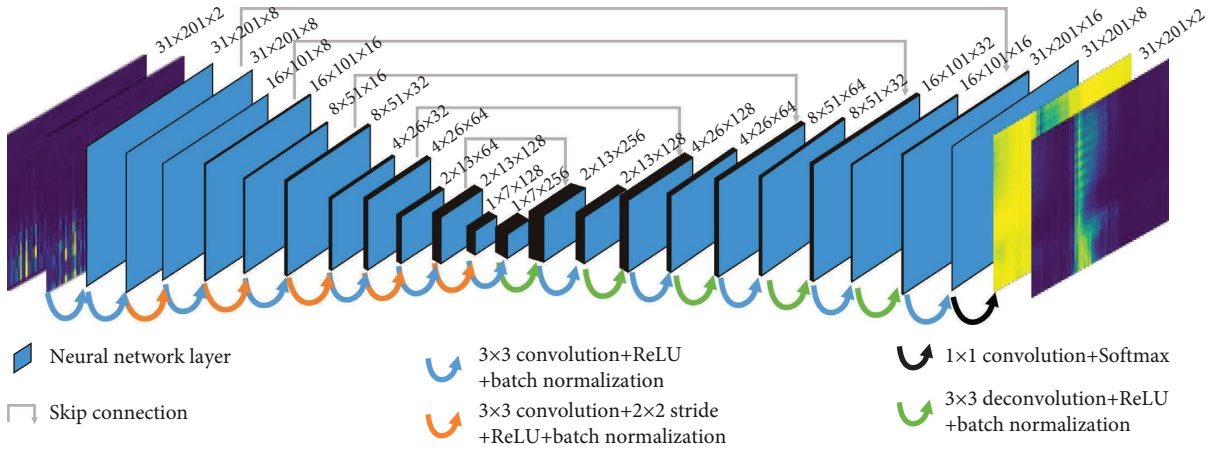

Figure 2: The network structure of the deep convolutional autoencoder.

to optimize the cross-entropy loss function to obtain optimal masks that separate the effective and noise signals. Meanwhile, in the convolutional autoencoder network structure, skip connections are utilized to improve the convergence of training and prediction [47]. Based on an autoencoder structure, the convolutional autoencoder performs convolutional operations instead of the inner product of ordinary matrices, which improves the feature extraction ability of the network and provides higher computational efficiency.

2.3. Denoising Framework Based on a Convolutional Autoencoder. For mine microseismic signal denoising, a denoising framework based on the deep convolutional autoencoder is constructed in this study, and the calculation process is shown in Figure 3.

First, in order to ensure the nonlinear expression ability of the constructed denoising framework and accelerate the convergence speed during network training, each noisy microseismic signal is normalized by subtracting its minimum value and dividing the resulting expression by the difference between its maximum and minimum values.

Then, all normalized signals are transformed into the time-frequency domain using the short-time Fourier transform (STFT), and the real and imaginary parts of time-frequency coefficients serve as the input of the convolutional autoencoder to output the effective and noise signal masks. These masks are considered the targets in optimizing the convolutional autoencoder network during training. The loss function used in the network is the mean squared error loss, and the corresponding formula is as follows:

$$\text{Loss} = \frac{1}{2N}\sum\left\|\widehat{\mathbf{M}}_S(t,f) - \mathbf{M}_S(t,f)\right\|_2^2, \tag{7}$$

where N indicates the number of training samples, $\|\cdot\|_2$ represents the L2 norm, $\mathbf{M}_S(t,f)$ is the label (or mask) of an effective signal, and $\widehat{\mathbf{M}}_S(t,f)$ is the output of the convolutional autoencoder network (i.e., the predicted time-frequency mask of an effective signal).

Next, the effective and noise signal masks are applied to the time-frequency coefficient of each noisy microseismic signal, and the time-frequency coefficients of the potential effective signal $\widehat{\mathbf{S}}(t,f)$ and noise signal $\widehat{\mathbf{N}}(t,f)$ can be estimated according to the following formula:

$$\begin{cases} \widehat{\mathbf{S}}(t,f) = \widehat{\mathbf{M}}_S(t,f)\mathbf{Y}(t,f), \\ \widehat{\mathbf{N}}(t,f) = \widehat{\mathbf{M}}_N(t,f)\mathbf{Y}(t,f) \\ \quad = \left[1 - \widehat{\mathbf{M}}_S(t,f)\right]\mathbf{Y}(t,f). \end{cases} \tag{8}$$

Finally, inverse STFT is used to transform $\widehat{\mathbf{S}}(t,f)$ and $\widehat{\mathbf{N}}(t,f)$ to the time domain to obtain the final denoised effective and noise signals.

As can be seen from the entire computational process, the denoising framework based on the deep convolutional autoencoder considers microseismic signal denoising as separating the effective and noise signals. Taking the three-component noisy microseismic signals as the input and the time-frequency masks as the optimization targets, the denoising framework obtains the denoised effective and noise signals by applying the predicted masks to the noisy microseismic signals in the time-frequency domain. Instead of manually defining different features and thresholds to enhance the effective signals and attenuate the noise signals, it automatically learns rich features from training set to separate the effective and noise signals and realizes fast and automatic denoising. Therefore, the constructed denoising framework can reduce the effects of human parameter adjustment and threshold selection, accelerate the processing of microseismic data, and help the automation and intelligence of microseismic data processing.

3. Experiments and Results

To test the accuracy and efficiency of the constructed denoising framework, it was used to denoise real mine microseismic signals on the basis of analyzing the characteristics of noise signals. The results were compared with those obtained using WT and ensemble empirical mode decomposition (EEMD) to quantitatively evaluate the denoising effect of the constructed framework.

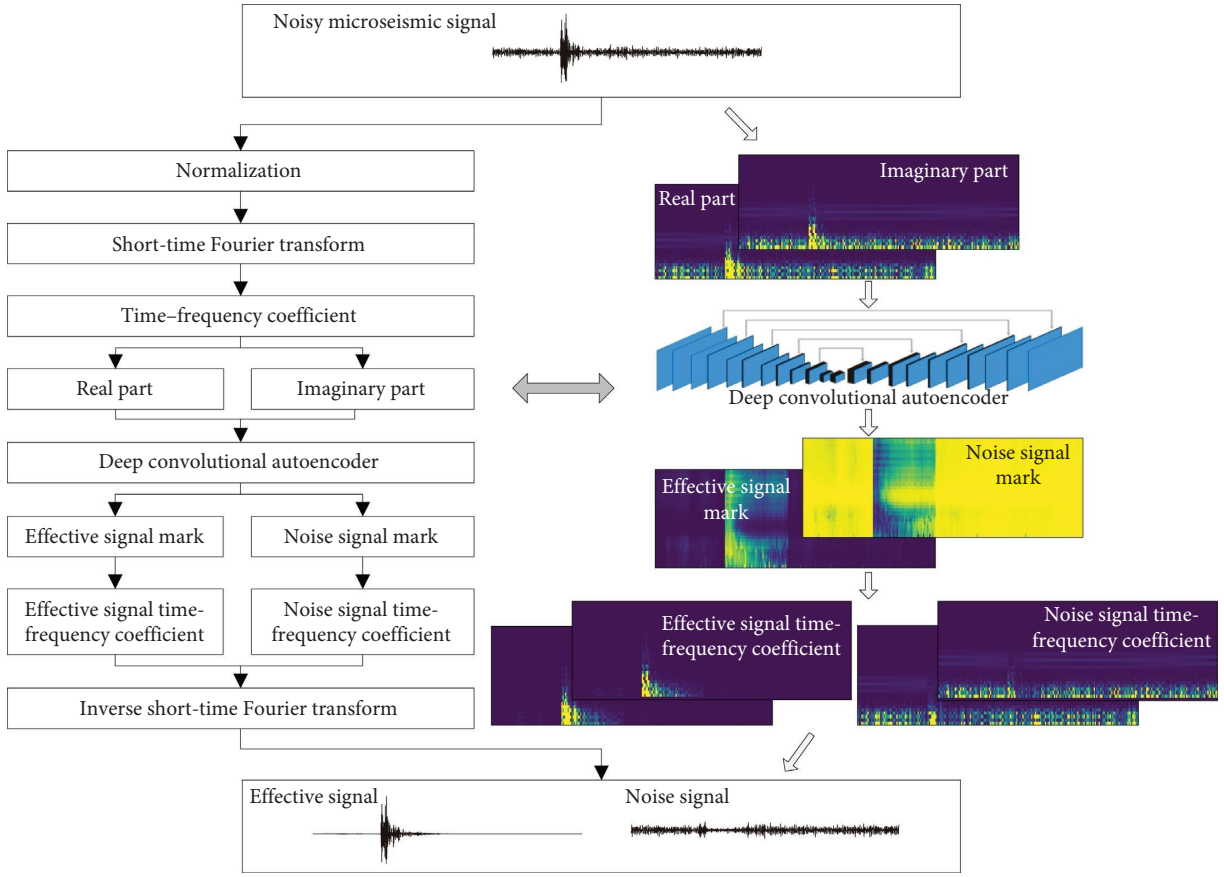

Figure 3: Denoising framework of mine microseismic signal based on the deep convolutional autoencoder.

3.1. Data. In order to demonstrate the denoising effect of the constructed framework, we took the microseismic monitoring signals of a mine in Gansu Province as an example. This mine is a copper-nickel sulfide mine with a mining depth of more than 1,000 m. As mining deepens, the mining conditions and operating environment deteriorate; particularly, the problem of dynamic disasters caused by rock mass excavation becomes more and more prominent, which further intensifies the difficulty of mining. Therefore, to analyze and predict dynamic disasters caused by the disturbance from deep mining and ensure the safety of mine operators' lives and properties, a set of microseismic monitoring system was set up for the mining area, and 16 three-component geophones (sampling rate is 1,000 Hz) were arranged to dynamically and continuously monitor various mine dynamic disasters, such as roof fall, collapse, and rock burst, in real time. The training and testing of the model require a large amount of sample data. However, clean effective microseismic signals cannot be obtained in practical application. Thus, this study selected 32,317 microseismic events with an extremely high SNR for clean effective microseismic signal samples and 51,251 non-microseismic event signals for noise signal samples and randomly combined these signals to generate noisy microseismic signals with different SNR levels. All the samples were randomly divided into training, validation, and test sets with proportions of 80%, 10%, and 10%, respectively. These sets were used to train the model, adjust the model hyperparameters, and test the denoising effect, respectively. Furthermore, 1,000 real mine microseismic signals with a low SNR were selected to test the generality of the model.

3.2. Analysis of Noise Signal Characteristics. Usually, signals received by a mine microseismic monitoring system can primarily be divided into three categories: effective microseismic signals, blast signals, and noise signals caused by various reasons [48]. Mining environments are complex, and various influencing factors lead to noise signals with a wide frequency band and rich spectrum components. The characteristics of various noise signals are clearly different in terms of waveform and spectrum. Even the same type of noise shows different characteristics owing to different generated conditions and environments [49]. Based on its source, noise can be roughly classified into the following types:

(1) Mechanical operation noise: It mainly refers to the noise generated by mine machinery and equipment, such as road headers, drills, and fans (Figure 4(i)). The frequency of this noise mostly lies in the range of 100–300 Hz, and the amplitude variation is small, mostly in the range of 10^{-7}–10^{-4} m/s; the waveforms are relatively dense, all of which are pulse burrs without clear attenuation and onset vibration. Being

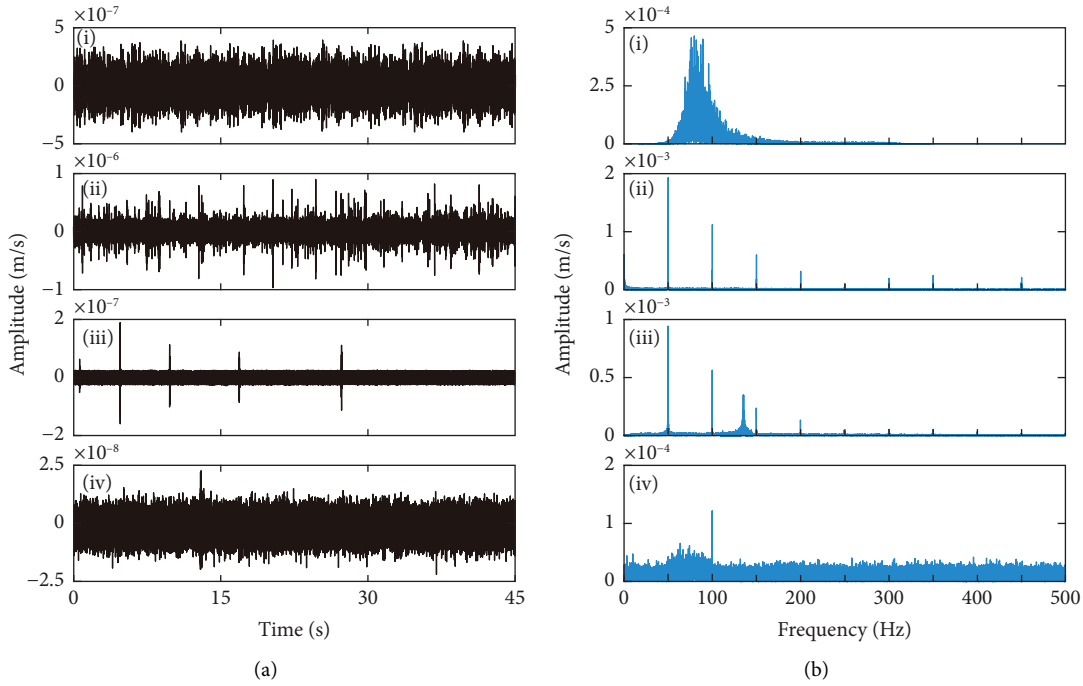

Figure 4: Several typical noise signals. (a) Noise signals (Z component) in the time domain. (b) Spectrogram of noise signals. (i) Mechanical interference signal. (ii) Electrical interference signal. (iii) Manmade knocking signal on the rock wall. (iv) Random noise signal.

related to the working time of machinery, its duration is generally long, reaching tens of seconds. Moreover, some noise signals are periodic.

(2) Electrical noise: It mainly refers to the electromagnetic interference generated by electrical equipment (e.g., fans, road headers, and other high-power mechanical equipment) in a mine and the electrical noise generated by cables and sensors (Figure 4(ii)). The frequency of this noise is relatively concentrated, with the main frequency being 50 Hz or an integer multiple of 50 Hz. The amplitude slightly changes, mostly in the range of 10^{-6}–10^{-4} m/s. Its waveform is generally in the shape of pulse burrs without clear onset vibration and attenuation, and the duration is also generally long.

(3) Human activity noise: It mainly refers to the noise generated by underground work, such as roadway repair, support, and manual equipment loading and unloading (Figure 4(iii)). This type of noise greatly changes in frequency range and amplitude; therefore, it is difficult to remove.

(4) Random noise: It mainly refers to the noise near sensors, including noise from external environments (e.g., from the mass caving, collapse, and spalling of rocks) or caused by instruments (Figure 4(iv)). The amplitude of this noise greatly varies, mostly in the range of 10^{-8}–10^{-3} m/s, and the frequency components are complex and distributed in high-, medium-, and low-frequency bands.

Generally, the complex waveform components of noise signals, various amplitudes, extremely irregular waveforms, and the complete spectrum aliasing of the noise and effective signals result in the effective microseismic signals being submerged into various noises, greatly increasing the difficulty of mine microseismic signal denoising.

3.3. Evaluation Indicators. Herein, three indicators, namely, SNR, correlation coefficient (CCR), and root mean squared error (RMSE), are used to quantitatively evaluate the denoising effect [50]. The formula for calculating the SNR is

$$\mathrm{SNR} = 10\log_{10}\left(\frac{\sigma_S}{\sigma_N}\right), \tag{9}$$

where σ_S is the standard deviation of an effective signal, while σ_N is that of a noise signal. The SNR represents the ratio of the effective signal to the noise signal in a noisy microseismic signal, and its unit is dB. It is a crucial indicator for evaluating signal quality. The larger the SNR, the lower the noise content and the better the denoising effect.

The formula for calculating the CCR is

$$\mathrm{CCR} = \frac{\mathrm{Cov}(\mathbf{X}, \mathbf{Y})}{\sqrt{\mathrm{Var}[\mathbf{X}]\mathrm{Var}[\mathbf{Y}]}}, \tag{10}$$

where $\mathbf{X}$ and $\mathbf{Y}$ represent the signals before and after denoising, respectively; $\mathrm{Cov}(\mathbf{X}, \mathbf{Y})$ represents the covariance of the signals before and after denoising; and $\mathrm{Var}[\mathbf{X}]$ and $\mathrm{Var}[\mathbf{Y}]$ represent the variance of the signals before and after

denoising, respectively. The CCR indicates the degree of correlation between the denoised signal and the clean effective microseismic signal. Its value is between 0 and 1. The closer the value is to 1, the more similar the signal waveform is to the ideal signal waveform and the better the denoising effect is.

The formula for calculating the RMSE is

$$\mathrm{RMSE} = \sqrt{\frac{1}{n}\|\mathbf{X} - \mathbf{Y}\|_2^2}, \tag{11}$$

where $\|\cdot\|_2$ represents the L2 norm; $\mathbf{X}$ and $\mathbf{Y}$ represent the signals before and after denoising, respectively; and n is the number of signal sampling points. The RMSE is the evaluation indicator for the deviation of the denoised signal from the mean value of the clean effective microseismic signal. Similar to the CCR, the smaller the value is, the closer the denoised signal is to the ideal signal and the better the denoising effect is.

3.4. Results and Discussion. The test environment included Intel(R) Core(TM) i7-8550U CPU @ 1.80 GHz, 16.0 GB RAM, and NVIDIA GeForce MX150 graphics card, with a Microsoft Windows 10 Home 64 bit operating system, Python 3.7.10, and TensorFlow 2.3.0. The experiment with the constructed denoising framework in this study was divided into two stages: model training and model denoising. In the model training stage, the effective and noise signals were used as input, and corresponding labels, the effective and noise signal masks, were used as the target output of the network. The cross-entropy loss function was used to calculate the distance between the output masks and labels, while the stochastic gradient descent algorithm was used to minimize the loss function. For the convenience of training, the sampling rate of the mine microseismic signals was resampled from 1,000 to 250 Hz. After repeated training and tuning experiments, the error of the training result was minimized (i.e., the training of the model was completed). The model training results are presented in Figure 5.

As shown in Figure 5, the average value of the cross-entropy loss function gradually decreased with an increase in the number of epochs during the model training, which showed a clear convergence trend. Moreover, the convergence speed of the model was fast. After 100 epochs of training, the average value of the cross-entropy loss function no longer decreased, and the model became stable.

After the model training was completed, it entered the model denoising stage. In this stage, the noisy microseismic signals were input into the model, and the separated effective and noise signals were output to realize the denoising of mine microseismic signals. In order to test the denoising effect of the proposed method, the noise and effective signals were combined into noisy microseismic signals with different SNR levels to form a test set for model testing. Furthermore, to quantitatively analyze the denoising effect of the proposed method, the denoising results of two common denoising methods, WT and EEMD, were compared with the processing results of the method based on the deep convolutional autoencoder. The experimental results of denoising under different SNR levels (from −6 to 8 dB) are presented in Table 1 and Figure 6.

In Figure 6, (i) and (ii) represent the clean effective and noise signals, respectively, (iii) represents noisy microseismic signals, and (iv) and (v) represent the denoising results obtained using the proposed method, namely, the effective microseismic and noise signals. Figure 6 illustrates two denoising examples. For the first one (Figures 6(a) and 6(b)), the SNR, CCR, and RMSE before denoising are −4.07, 0.68, and 11.43, respectively, while these values improve to 6.95, 0.86, and 6.08, respectively, after denoising. For the other one (Figures 6(c) and 6(d)), the SNR, CCR, and RMSE are −0.94, 0.79, and 8.55, respectively, before denoising, and 8.93, 0.90, and 5.27, respectively, after denoising. Taking Figures 6(a) and 6(b) as an example, on the one hand, the time-frequency planes before and after denoising (Figure 6(a)) show that the energy of low- and high-frequency noise was completely suppressed after denoising in two time periods of approximately 0 to 20.96 s and 24.12 to 45 s, whereas the energy of effective microseismic signal was clearly evident in 20.96 to 24.12 s. Meanwhile, some low-frequency noises around the effective signal were suppressed to varying degrees. Based on the whole time-frequency plane (Figure 6(a)(iv)), only the effective signal part of the microseismic signal had energy, showing that the proposed method had achieved a satisfactory noise suppression of the mine microseismic signal. On the other hand, it can be seen intuitively from the time-domain planes (Figure 6(b)) that the proposed method could effectively remove the noise in the mine microseismic signal and restore the effective microseismic signal.

WT and EEMD are two common methods in mine microseismic signal denoising. The basic principle of WT is that after a microseismic signal is decomposed by the Mallat algorithm, the wavelet coefficient amplitude of the effective signal is greater than that of the noise signal. If an appropriate threshold is selected to remove the wavelet coefficient smaller than the threshold and retain those greater than the threshold, the denoising task can be completed [51, 52]. To achieve the best denoising effect for WT, repeated tests were conducted. The results show that when the db4 wavelet basis function is used, the number of layers in the wavelet decomposition is set to five, and when the Heursure threshold function is adopted [53], the denoising effect is the best. EMD is based on the Hilbert–Huang transform to decompose a microseismic signal into a sum of IMFs. The noise signal is mainly concentrated in high-frequency components (low-sequence IMFs), while the effective signal is mainly concentrated in low-frequency components (high-sequence IMFs). Therefore, reconstruction using low-frequency IMFs can achieve the purpose of denoising [54, 55]. Although EMD decomposes each signal according to its time-scale characteristics without presetting any basis functions, modal aliasing is prone to appear. EEMD utilizes the uniform distribution and zero-mean characteristics of white noise spectrum to solve the problem of modal aliasing in EMD by adding white noise and averaging it multiple times [19]. According to the test results, twelve IMFs are generated after a microseismic signal is adaptively decomposed using

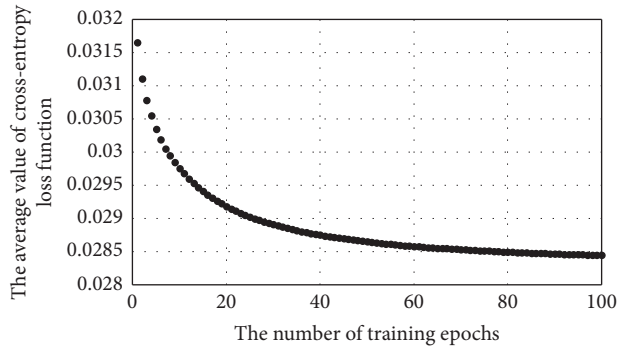

Figure 5: Graph of the relationship between the average value of the cross-entropy loss function and the number of epochs during the model training.

Table 1: Comparison of different denoising methods.

SNR levels (dB)	WT			EEMD			Our method		
	SNR	CCR	RMSE	SNR	CCR	RMSE	SNR	CCR	RMSE
−6	0.35	0.54	15.14	0.72	0.58	14.23	3.59	0.70	9.38
−5	0.94	0.59	13.73	1.29	0.61	13.15	4.27	0.73	8.13
−4	1.72	0.64	12.25	1.91	0.65	11.76	5.27	0.77	7.25
−3	2.42	0.69	11.02	2.74	0.72	10.99	5.93	0.79	6.84
−2	3.01	0.74	9.77	3.50	0.78	9.44	6.68	0.82	6.24
−1	3.89	0.78	8.94	4.26	0.80	8.12	7.19	0.84	6.06
0	4.25	0.80	8.16	4.98	0.82	7.59	7.75	0.87	5.74
1	5.01	0.81	7.65	5.78	0.84	7.02	8.36	0.89	5.45
2	5.73	0.84	6.99	6.38	0.85	6.67	8.94	0.91	5.04
3	6.52	0.86	6.54	7.43	0.87	6.08	9.35	0.92	4.80
4	7.24	0.90	5.98	8.20	0.91	5.36	9.82	0.93	4.38
5	8.16	0.91	5.37	8.89	0.92	5.11	10.53	0.93	3.91
6	8.93	0.92	5.03	9.33	0.93	4.93	11.23	0.95	3.54
7	9.47	0.93	4.84	9.97	0.94	4.26	12.01	0.95	2.99
8	10.55	0.94	4.37	10.65	0.95	4.18	12.87	0.96	2.27

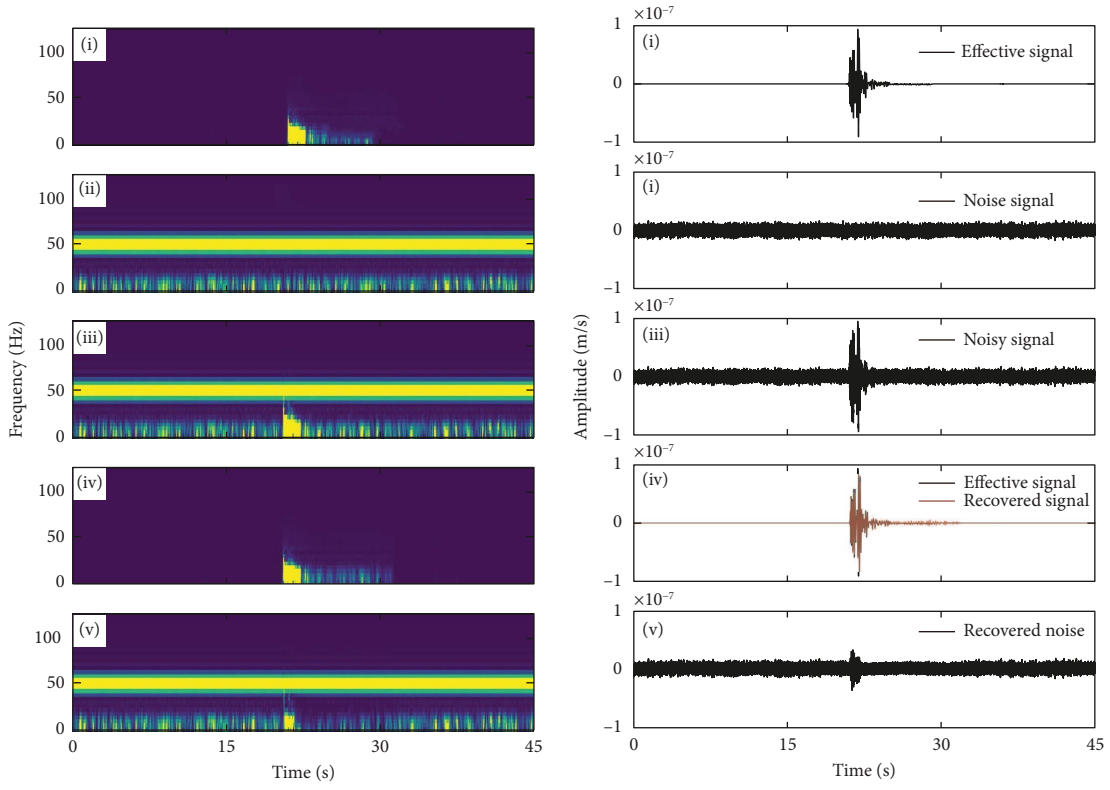

Figure 6: Continued.

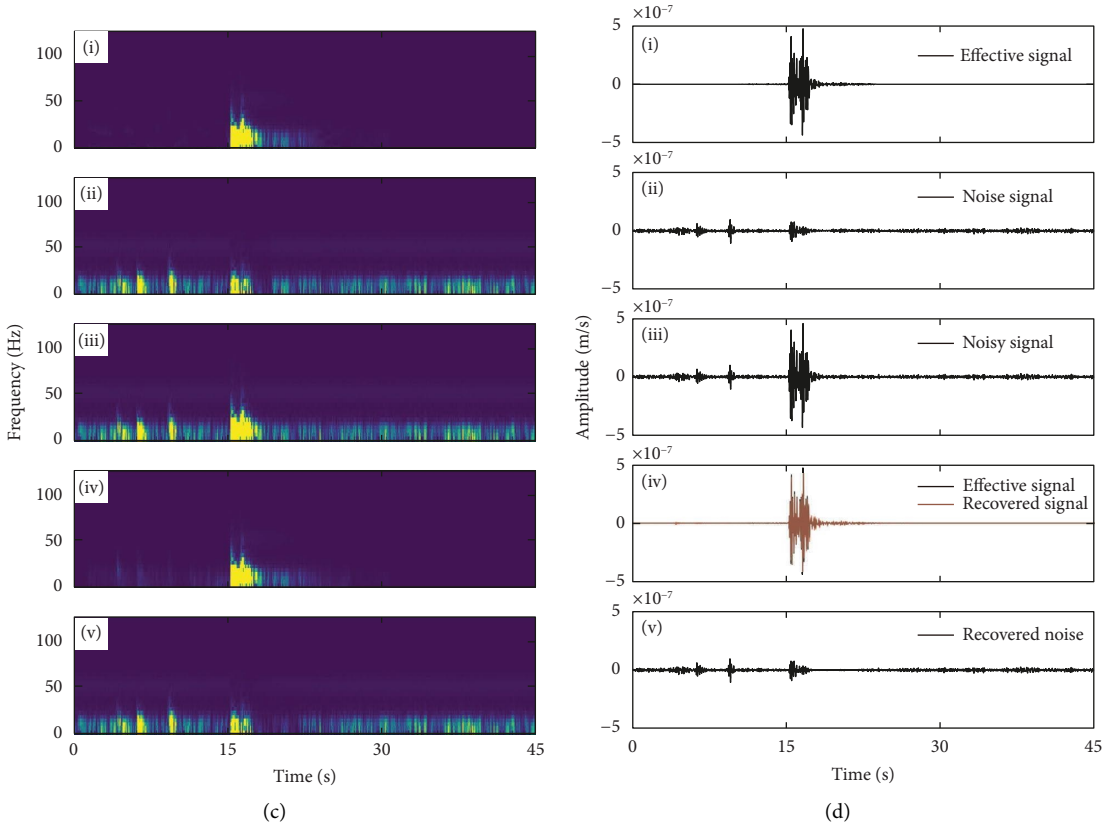

Figure 6: Denoising examples. (a, c) The effective signals (Z component) in the time-frequency domain. (b, d) The effective signals (Z component) in the time domain. The time-frequency coefficients and waveforms of the effective, noise, and noisy microseismic signals are plotted in panels (i), (ii), and (iii), respectively. The recovered effective signals in the time-frequency domain and their time-domain waveforms are shown in panels (a, c) (iv) and (b, d) (iv), respectively. Panels (a, c) (v) and (b, d) (v) show the recovered noise signals in the time-frequency domain and their time-domain waveforms, respectively.

EEMD. Among them, the first six IMFs are noisy components, and the energy ratio of the last six IMFs is much higher than that of others, which contain more information about the effective microseismic event. Therefore, the denoising task can be completed well by extracting the last six IMFs to reconstruct the effective microseismic signal. Table 1 and Figure 6 show that although WT and EEMD can improve the SNR of each microseismic signal to a certain extent, the degree of improvement is limited. However, the proposed method can learn the characteristics of the effective and noise signals through training, and the SNR of each effective microseismic signal after denoising is higher. Moreover, the CCR exhibits considerable improvement at different SNR levels, and the corresponding RMSE is smaller. The higher SNR and CCR and the smaller RMSE indicate that the proposed method has a strong denoising ability and a small degree of waveform distortion after denoising, which is close to the ideal signal. The experimental results show that the overall SNR for the proposed method is considerably improved, CCR is substantially improved, RMSE is smaller, and denoising ability is the best compared with those for WT and EEMD. In addition, the more serious the microseismic signal pollution is, the more obvious the denoising advantage of our method is.

To visually demonstrate the overall denoising effect of the constructed framework, the statistical histograms of the SNR, CCR, and RMSE for the test set before and after denoising are presented in Figure 7. It can be clearly seen from Figure 7(a) that the SNR for the test set before denoising is mainly distributed between −5.99 and 7.92 dB, with the average SNR being 1.03 dB. The SNR after denoising is mainly distributed between −1.94 and 13.77 dB, with the average SNR being 5.68 dB. Therefore, the average SNR of the denoised signals is considerably improved. As shown in Figure 7(b), the CCR before denoising is mainly between 0.51 and 0.78, with an average of 0.65. The number of noisy microseismic signals distributed in each interval of the CCR is relatively uniform. After denoising, the CCR is mainly between 0.63 and 0.98, the number of denoised microseismic signals in each interval of the CCR gradually increases with an increase of its value, and the average CCR after denoising is 0.92. These findings indicate that the denoised microseismic signals can effectively preserve the corresponding waveforms of the effective signals. In Figure 7(c), the RMSE for the test set before denoising is mainly distributed between 5.12 and 15.87, whose average RMSE is 10.43. The RMSE after denoising is mainly distributed between 1.25 and 9.76, whose average RMSE is 4.98. The RMSE is greatly

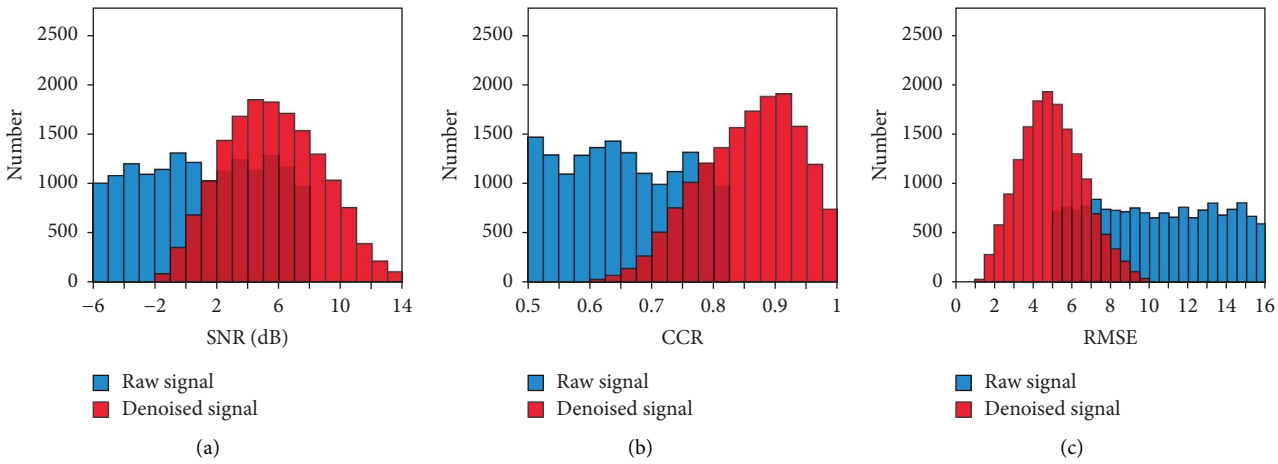

Figure 7: Statistical histograms of the denoising effect for the test set. (a) Statistical histograms of the SNR before and after denoising. (b) Statistics histograms of the CCR before and after denoising. (c) Statistical histograms of the RMSE before and after denoising.

reduced after denoising, indicating closeness to the ideal signal.

The denoising framework based on the convolutional autoencoder was trained on synthetic microseismic data that superimposed the real noise signals on the real high-SNR effective microseismic signals. To test the generality of the constructed denoising framework, we applied it to 1,000 real mine microseismic signals. These signals (Figure 8(i)) are severely polluted by noise, and the SNR is low. Moreover, to intuitively compare the denoising results of the proposed method with those of other methods, we used the constructed framework, WT, and EEMD to denoise mine microseismic signals with different SNR levels. The comparison is presented in Figure 8.

Figure 8 presents the denoising results of different methods under different SNR levels. As can be seen from (iv) and (v) in Figure 8, at a high-SNR level, WT and EEMD can achieve a relatively good denoising effect, and the waveform distortion is relatively small. However, with the decrease in the SNR of mine microseismic signals, the denoising ability of WT and EEMD gradually decreases. Although the denoising effect of EEMD is better than that of WT, the denoising results of these two methods still contain much noise, the distortion of waveforms after denoising is large, and the denoising effect is poor. In comparison, the denoising effect of the proposed method is obviously better, and the overall waveform of each effective microseismic signal after denoising is clearer. After denoising, the P- and S-waves of each effective microseismic signal are more obvious, leading to better recognition of P- and S-wave phases. In particular, the noise before the arrival of P-wave is well suppressed, and the noise residue is approximately zero (Figure 8(iii)), which is beneficial for accurately detecting microseismic events and phases in the subsequent microseismic data processing. The experimental results show that even in the case of a low SNR, the proposed method can better suppress the noise in mine microseismic signals and realize the separation of the effective and noise signals. Therefore, although our method is trained on synthetic data, it can be generalized to practical denoising tasks and applied to the denoising of real mine microseismic signals. Moreover, it does not require any prior knowledge or preprocessing and has strong practicability.

In real mine microseismic signal processing, given the extended period of microseismic monitoring and the numerous data involved, computational efficiency also represents a key concern for denoising methods. To evaluate the computational efficiency of the constructed denoising framework, we recorded the time taken by the proposed method to process different number of microseismic signals and compared them with those of WT and EEMD. The results are presented in Table 2 and Figure 9. As can be seen from the comparison (Table 2 and Figure 9), our method takes a far shorter time to denoise microseismic signals, and this merit will become even more prominent with an increase in the data processed. Of course, as our method is a supervised learning method, the model has to be trained before use—in our experiment, it takes approximately 9,627 s to train the model on the constructed training samples—but once the model is trained, it denoises signals efficiently and quickly.

In summary, the common denoising methods of mine microseismic signals, such as WT and EEMD, can improve the quality of signals to a certain extent, but the ability to denoise is limited, especially under a low-SNR condition. Moreover, in practical application, these methods generally require more manual participation, which greatly limits their application scope. For instance, to have a good denoising effect, WT needs to select the best basis function and decomposition layer according to the real signals. Although EEMD solves the problem of signal distortion caused by modal aliasing in EMD and does not need to preset any basis functions, it requires multiple iterations during decomposition, which is very time-consuming. Furthermore, there is a lack of uniform criteria for stopping iterations, and different conditions may lead to different results. By comparison, instead of manually defining different features and thresholds to improve the SNR, our data-driven method can

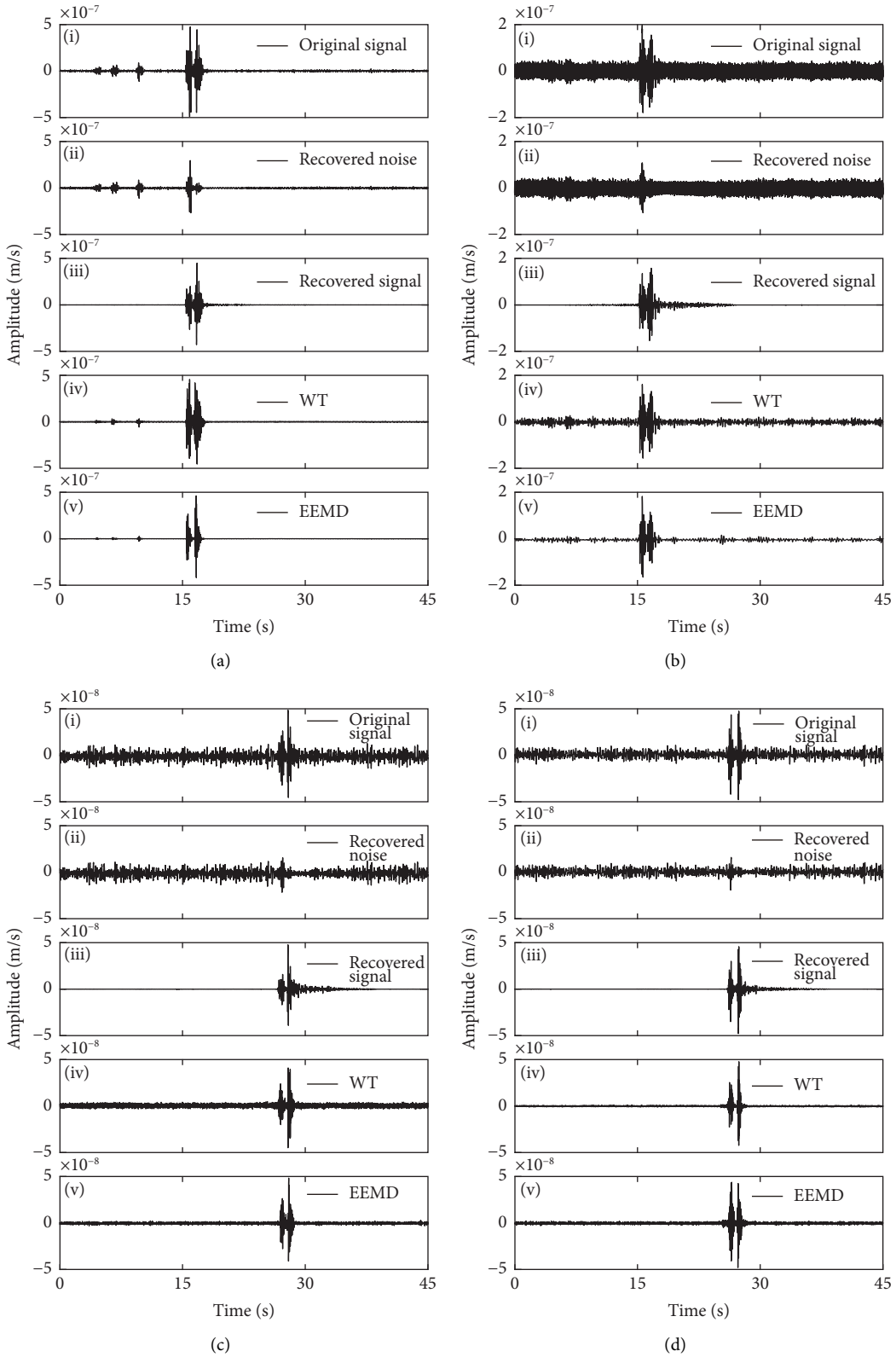

Figure 8: Comparison of denoising results. (a–d) Denoising results of different signals. (i) Original mine microseismic signals (Z component). (ii) Recovered noise signals with the proposed method. (iii) Recovered effective signals with the proposed method. (iv) The results of WT. (v) The results of EEMD.

Table 2: Processing time of different methods.

Number of test samples	Time by WT (s)	Time by EEMD (s)	Time by our method (s)
1,000	45	105	31
2,000	91	209	61
5,000	228	557	154
10,000	457	1,173	335
20,000	974	2,406	786
50,000	3,106	7,695	2,482

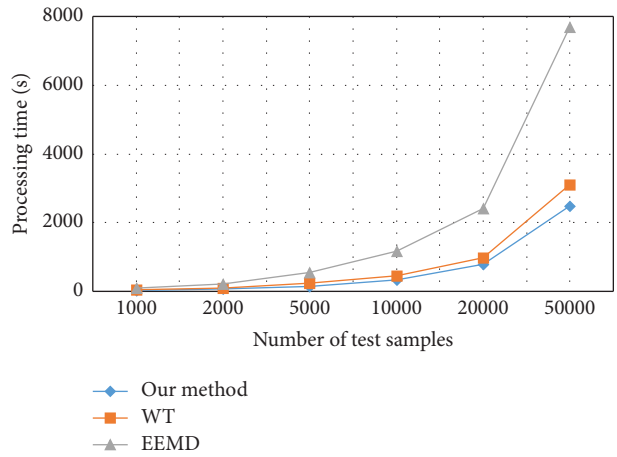

Figure 9: Processing time of different methods.

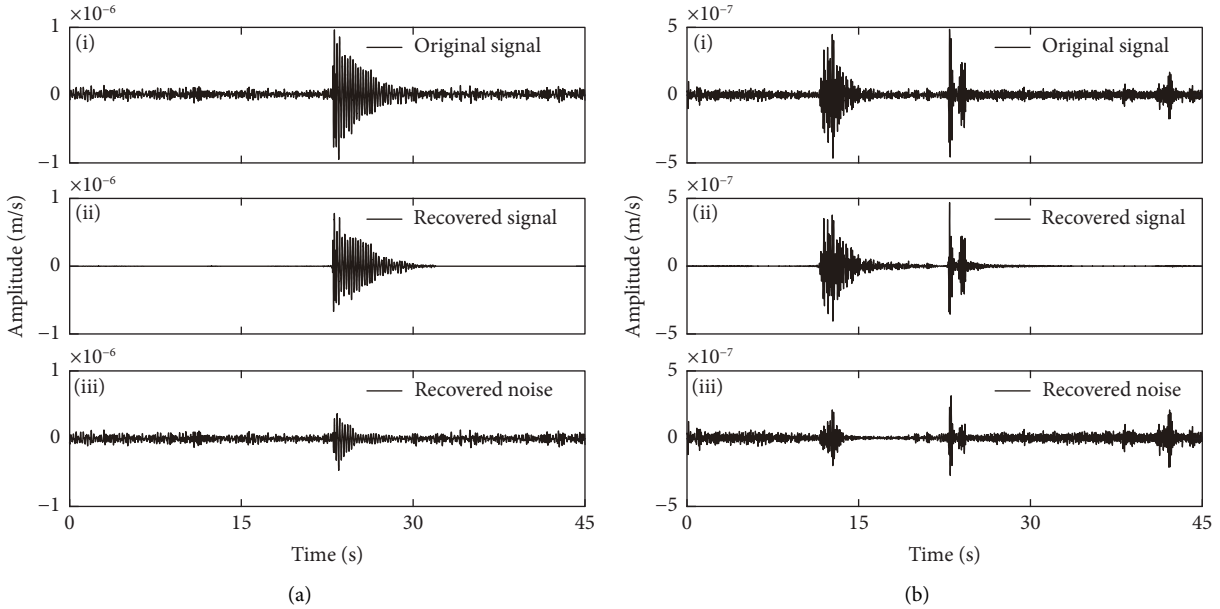

Figure 10: Denoising results of blasting signals (Z component). The waveforms of blasting signals, recovered effective blasting, and noise signals are plotted in panels (i), (ii), and (iii), respectively.

automatically learn rich features from synthetic data to separate the effective and noise signals and realize fast and automatic denoising. The performance, denoising effect and computational efficiency, of the constructed framework outperforms these two denoising methods even in the case of a low SNR. As a supervised learning method, it has to be trained before use, and the quality and quantity of training data will influence the denoising effect. It is sometimes difficult to obtain large, diverse, and reliable training samples in practical application. Using microseismic signals with a high SNR instead of clean effective signals to train the model will more or less bring some interference to it and

affect its generality. This may be the main reason why the waveform amplitude preservation of the denoised signal is not so great. In the process of denoising, our method applies the predicted masks to noisy microseismic signals in the time-frequency domain to separate the effective and noise signals. Because the range of the value for each mask is between 0 and 1, the constructed denoising framework cannot recover a signal with the value larger than that of the input noisy microseismic signal.

Blasting is a common construction method in mining. Despite providing convenience for mining, it may cause some potential hazards. Therefore, researching blasting signals has a crucial engineering application value. To accurately extract the subsequent blasting features, each blasting signal first needs to be denoised. The source of blast signals is of an expansive type. The energy generated is instantaneously released, compressing the surrounding rock masses and primarily propagating outwards in the form of a P-wave. This type of signal has a high energy and large waveform amplitude. Its waveform decays fast at the beginning and slows down later, forming a "dovetail" waveform shape. The duration of blast signal is generally longer than that of effective microseismic signal (rock rupture signal). When making the model training set, we also added a certain number of blasting signals so that the constructed framework can also denoise blasting signals. The denoising results of blasting signals are presented in Figure 10. The blasting signal waveforms after denoising using the constructed framework are obvious, the characteristics of "dovetail" waveforms are clear (Figure 10(ii)), noise is well suppressed, and blasting events can be effectively distinguished.

4. Conclusion

Microseismic monitoring is an integral part of mine safety management and an effective means to realize mine dynamic disaster monitoring and early warning. Microseismic signal denoising is a basic and crucial link in data processing, which influences the accuracy and reliability of the monitoring system. Therefore, to address the denoising problem of mine microseismic signals, a denoising framework based on a deep convolutional autoencoder was constructed in this study. The constructed denoising framework can learn the sparse representations of the input signals in the time-frequency domain and generate two separate masks for each noisy microseismic signal based on these representations to extract the corresponding signals (one is used to extract the effective signal, while the other is used to extract the noise signal), thereby achieving the purpose of fast and automatic denoising. To verify the effectiveness of the denoising framework, we applied it to real mine microseismic signals and compared the denoising results with those of two methods. The experimental results show that the denoising framework can considerably improve the SNR of each microseismic signal as well as reduce its waveform distortion degree after denoising. Compared with WT and EEMD, even in the case of a low SNR, the denoising framework can better suppress the noise in mine microseismic signals, preserve the waveform shape of effective signals to the greatest extent, and efficiently separate the effective and noise signals. Moreover, the constructed denoising framework does not need to understand and identify the complex relationship between attributes. Because it does not require any prior knowledge or preprocessing and has strong practicability, the denoising framework can also be utilized for microseismic monitoring signals in other fields, such as for the stability monitoring of surrounding rocks in tunnel excavations and chamber surrounding rocks in hydropower stations.

Data Availability

Some or all data, models, and codes used in this study are available from the corresponding author upon request.

Conflicts of Interest

The authors declare that they have no conflicts of interest.

Acknowledgments

This work was supported by the Department of Science and Technology of Sichuan Province (grant no. 2022YFS0521) and National Natural Science Foundation of Sichuan Province (grant no. 2023NSFSC0020).

References

[1] M. G. Zhai, R. Z. Hu, Y. Wang et al., "Mineral resource science in China: review and perspective," *Geography and Sustainability*, vol. 2, no. 2, pp. 107–114, 2021.

[2] J. Lu, D. M. Zhang, G. Huang, X. Li, H. Gao, and G. Z. Yin, "Effects of loading rate on the compound dynamic disaster in deep underground coal mine under true triaxial stress," *International Journal of Rock Mechanics and Mining Sciences*, vol. 134, Article ID 104453, 2020.

[3] X. X. Zhou, Z. H. Ouyang, R. R. Zhou et al., "An approach to dynamic disaster prevention in strong rock burst coal seam under multi-aquifers: a case study of Tingnan coal mine," *Energies*, vol. 14, no. 21, Article ID 14217287, 2021.

[4] L. M. Qiu, Y. J. Tong, J. Li, D. Z. Song, M. Wang, and S. Yin, "An experimental study: variation law of magnetic field around concrete during loading," *Minerals*, vol. 12, no. 4, Article ID 12040399, 2022.

[5] M. B. Zhu, J. Y. Cheng, and Z. Zhang, "Quality control of microseismic P-phase arrival picks in coal mine based on machine learning," *Computers & Geosciences*, vol. 156, Article ID 104862, 2021.

[6] G. F. Liu, X. T. Feng, G. L. Feng, B. R. Chen, D. F. Chen, and S. Q. Duan, "A method for dynamic risk assessment and management of rockbursts in drill and blast tunnels," *Rock Mechanics and Rock Engineering*, vol. 49, no. 8, pp. 3257–3279, 2016.

[7] X. L. Li, S. J. Chen, E. Y. Wang, and Z. H. Li, "Rockburst mechanism in coal rock with structural surface and the microseismic (MS) and electromagnetic radiation (EMR) response," *Engineering Failure Analysis*, vol. 124, Article ID 105396, 2021.

[8] N. Y. Lan and F. C. Zhang, "Seismic data recovery using deep targeted denoising priors in an alternating optimization framework," *Geophysics*, vol. 87, no. 4, pp. 279–291, 2022.

[9] Y. Li, L. L. Li, and C. Zhang, "Desert seismic signal denoising by 2D compact variational mode decomposition," *Journal of*

Geophysics and Engineering, vol. 16, no. 6, pp. 1048–1060, 2019.

[10] S. M. Mousavi and C. A. Langston, "Adaptive noise estimation and suppression for improving microseismic event detection," *Journal of Applied Geophysics*, vol. 132, pp. 116–124, 2016.

[11] S. M. Mousavi and C. A. Langston, "Hybrid seismic denoising using higher-order statistics and improved wavelet block thresholding," *Bulletin of the Seismological Society of America*, vol. 106, no. 4, pp. 1380–1393, 2016.

[12] S. M. Mousavi and C. A. Langston, "Automatic noise-removal/signal-removal based on general cross-validation thresholding in synchrosqueezed domain and its application on earthquake data," *Geophysics*, vol. 82, no. 4, pp. 211–227, 2017.

[13] G. A. Tselentis, N. Martakis, P. Paraskevopoulos, A. Lois, and E. Sokos, "Strategy for automated analysis of passive microseismic data based on s-transform, otsu's thresholding, and higher order statistics," *Geophysics*, vol. 77, no. 6, pp. 43–54, 2012.

[14] G. Tang and J. W. Ma, "Application of total-variation-based curvelet shrinkage for three-dimensional seismic data denoising," *IEEE Geoscience and Remote Sensing Letters*, vol. 8, no. 1, pp. 103–107, 2011.

[15] H. Shan, J. W. Ma, and H. Z. Yang, "Comparisons of wavelets, contourlets and curvelets in seismic denoising," *Journal of Applied Geophysics*, vol. 69, no. 2, pp. 103–115, 2009.

[16] B. F. Wang, R. S. Wu, X. H. Chen, and J. Y. Li, "Simultaneous seismic data interpolation and denoising with a new adaptive method based on dreamlet transform," *Geophysical Journal International*, vol. 201, no. 2, pp. 1182–1194, 2015.

[17] C. Zhang and M. van der Baan, "Multicomponent microseismic data denoising by 3d shearlet transform," *Geophysics*, vol. 83, no. 3, pp. 45–51, 2018.

[18] W. Chen, J. Y. Xie, S. H. Zu, S. W. Gan, and Y. K. Chen, "Multiple-reflection noise attenuation using adaptive randomized-order empirical mode decomposition," *IEEE Geoscience and Remote Sensing Letters*, vol. 14, no. 1, pp. 18–22, 2017.

[19] J. J. Han and M. van der Baan, "Microseismic and seismic denoising via ensemble empirical mode decomposition and adaptive thresholding," *Geophysics*, vol. 80, no. 6, pp. 69–80, 2015.

[20] S. Gaci, "The use of wavelet-based denoising techniques to enhance the first-arrival picking on seismic traces," *IEEE Transactions on Geoscience and Remote Sensing*, vol. 52, no. 8, pp. 4558–4563, 2014.

[21] X. Li, L. L. Dong, B. Li, Y. Y. Lei, and N. W. Xu, "Microseismic signal denoising via empirical mode decomposition, compressed Sensing, and soft-thresholding," *Applied Sciences*, vol. 10, no. 6, Article ID 10062191, 2020.

[22] R. Anvari, M. A. Nazari Siahsar, S. Gholtashi, A. Roshandel Kahoo, and M. Mohammadi, "Seismic random noise attenuation using synchrosqueezed wavelet transform and low-rank signal matrix approximation," *IEEE Transactions on Geoscience and Remote Sensing*, vol. 55, no. 11, pp. 6574–6581, 2017.

[23] R. Anvari, A. R. Kahoo, M. Mohammadi, N. A. Khan, and Y. K. Chen, "Seismic random noise attenuation using sparse low-rank estimation of the signal in the time–frequency domain," *Ieee Journal of Selected Topics in Applied Earth Observations and Remote Sensing*, vol. 12, no. 5, pp. 1612–1618, 2019.

[24] H. Liu, W. D. Wang, C. L. Xiang, L. J. Han, and H. Z. Nie, "A de-noising method using the improved wavelet threshold function based on noise variance estimation," *Mechanical Systems and Signal Processing*, vol. 99, no. 15, pp. 30–46, 2018.

[25] X. X. Gao, X. X. Pan, and G. A. Zhu, "An analysis method for time-frequency-and energy-domain characteristics of downhole microseismic signals and its application," *Shock and Vibration*, vol. 2021, Article ID 6699221, 12 pages, 2021.

[26] A. Gholami, "Sparse time–frequency decomposition and some applications," *IEEE Transactions on Geoscience and Remote Sensing*, vol. 51, no. 6, pp. 3598–3604, 2013.

[27] W. K. Lu and F. Y. Li, "Seismic spectral decomposition using deconvolutive short-time Fourier transform spectrogram," *Geophysics*, vol. 78, no. 2, pp. 43–51, 2013.

[28] N. Iqbal, E. T. Liu, J. H. McClellan, A. Al-Shuhail, S. I. Kaka, and A. Zerguine, "Detection and denoising of microseismic events using time–frequency representation and tensor decomposition," *IEEE Access*, vol. 6, pp. 22993–23006, 2018.

[29] D. Zhang, Z. Y. Zeng, Y. Q. Shi et al., "An effective denoising method based on cumulative distribution function thresholding and its application in the microseismic signal of a metal mine with high sampling rate (6 kHz)," *Frontiers in Earth Science*, vol. 10, Article ID 933284, 2022.

[30] Z. Y. Zeng, T. X. Lu, P. Han et al., "Microseismic data denoising in the sychrosqueezed domain by integrating the wavelet coefficient thresholding and pixel connectivity," *Geophysical Journal International*, vol. 232, no. 2, pp. 1113–1128, 2022.

[31] N. Iqbal, A. Zerguine, S. Kaka, and A. Al-Shuhail, "Automated SVD filtering of time–frequency distribution for enhancing the SNR of microseismic/microquake events," *Journal of Geophysics and Engineering*, vol. 13, no. 6, pp. 964–973, 2016.

[32] W. Liu, S. Y. Cao, and Y. K. Chen, "Seismic time–frequency analysis via empirical wavelet transform," *IEEE Geoscience and Remote Sensing Letters*, vol. 13, no. 1, pp. 28–32, 2016.

[33] S. M. Mousavi, C. A. Langston, and S. P. Horton, "Automatic microseismic denoising and onset detection using the synchrosqueezed continuous wavelet transform," *Geophysics*, vol. 81, no. 4, pp. 341–355, 2016.

[34] Q. K. Feng and Y. Li, "Denoising deep learning network based on singular spectrum analysis—DAS seismic data denoising with multichannel SVDDCNN," *IEEE Transactions on Geoscience and Remote Sensing*, vol. 60, pp. 1–11, 2022.

[35] I. Vera Rodriguez, D. Bonar, and M. Sacchi, "Microseismic data denoising using a 3C group sparsity constrained time–frequency transform," *Geophysics*, vol. 77, no. 2, pp. 21–29, 2012.

[36] X. W. Wang and H. Z. Wang, "Application of sparse time–frequency decomposition to seismic data," *Applied Geophysics*, vol. 11, no. 4, pp. 447–458, 2014.

[37] Z. L. Liu, Y. Q. Jin, M. J. Zuo, and Z. P. Feng, "Time-frequency representation based on robust local mean decomposition for multicomponent AM-FM signal analysis," *Mechanical Systems and Signal Processing*, vol. 95, pp. 468–487, 2017.

[38] N. Iqbal, "Deepseg: deep segmental denoising neural network for seismic data," *IEEE Transactions on Neural Networks and Learning Systems*, vol. 34, no. 7, pp. 3397–3404, 2023.

[39] A. Othman, N. Iqbal, S. M. Hanafy, and U. B. Waheed, "Automated event detection and denoising method for passive seismic data using residual deep convolutional neural networks," *IEEE Transactions on Geoscience and Remote Sensing*, vol. 60, pp. 1–11, 2021.

[40] Y. X. Zhao, Y. Li, and B. J. Yang, "Denoising of seismic data in desert environment based on a variational mode decomposition and a convolutional neural network," *Geophysical Journal International*, vol. 221, no. 2, pp. 1211–1225, 2020.

[41] W. Q. Zhu, S. M. Mousavi, and G. C. Beroza, "Seismic signal denoising and decomposition using deep neural networks," *IEEE Transactions on Geoscience and Remote Sensing*, vol. 57, no. 11, pp. 9476–9488, 2019.

[42] X. T. Dong, T. Zhong, and Y. Li, "A deep-learning-based denoising method for multiarea surface seismic data," *IEEE Geoscience and Remote Sensing Letters*, vol. 18, no. 5, pp. 925–929, 2021.

[43] D. L. Donoho and I. M. Johnstone, "Ideal spatial adaptation by wavelet shrinkage," *Biometrika*, vol. 81, no. 3, pp. 425–455, 1994.

[44] K. G. Lore, A. Akintayo, and S. Sarkar, "LLNet: a deep autoencoder approach to natural low-light image enhancement," *Pattern Recognition*, vol. 61, pp. 650–662, 2017.

[45] K. Zhang, W. M. Zuo, Y. J. Chen, D. Y. Meng, and L. Zhang, "Beyond a Gaussian denoiser: residual learning of deep CNN for image denoising," *IEEE Transactions on Image Processing*, vol. 26, no. 7, pp. 3142–3155, 2017.

[46] P. S. Huang, M. Kim, M. Hasegawa-Johnson, and P. Smaragdis, "Joint optimization of masks and deep recurrent neural networks for monaural source separation," *IEEE/ACM Transactions on Audio, Speech, and Language Processing*, vol. 23, no. 12, pp. 2136–2147, 2015.

[47] O. Ronneberger, P. Fischer, and T. Brox, "U-Net: convolutional networks for biomedical image segmentation," in *Proceedings of the International Conference on Medical Image Computing and Computer-Assisted Intervention*, pp. 234–241, Springer, Cham, Switzerland, November 2015.

[48] Y. Li, T. H. Yang, H. L. Liu et al., "Real-time microseismic monitoring and its characteristic analysis in working face with high-intensity mining," *Journal of Applied Geophysics*, vol. 132, pp. 152–163, 2016.

[49] X. L. Li, Z. H. Li, E. Y. Wang et al., "Microseismic signal spectra, energy characteristics, and fractal features prior to rock burst: a case study from the Qianqiu coal mine, China," *Journal of Earthquake Engineering*, vol. 21, no. 6, pp. 891–911, 2017.

[50] J. Jenitta and A. Rajeswari, "An optimized baseline wander removal algorithm based on ensemble empirical mode decomposition," *IAENG International Journal of Computer Science*, vol. 42, no. 2, pp. 95–106, 2015.

[51] J. Li, Y. Li, Y. Li, and Z. H. Qian, "Downhole microseismic signal denoising via empirical wavelet transform and adaptive thresholding," *Journal of Geophysics and Engineering*, vol. 15, no. 6, pp. 2469–2480, 2018.

[52] Y. M. Kang, H. Y. Liu, M. M. A. Aziz, and K. A. Kassim, "A wavelet transform method for studying the energy distribution characteristics of microseismicities associated rock failure," *Journal of Traffic and Transportation Engineering*, vol. 6, no. 6, pp. 631–646, 2019.

[53] D. Zhang, H. B. Zhao, and J. K. Yang, "Signal denoising of double-beam and double-scattering laser Doppler velocimetry based on wavelet layering," *Optik*, vol. 202, Article ID 163545, 2020.

[54] N. E. Huang, Z. Shen, S. R. Long et al., "The empirical mode decomposition and the Hilbert spectrum for nonlinear and nonstationary time series analysis," *Proceedings of the Royal Society of London. Series A: Mathematical, Physical and Engineering Sciences*, vol. 454, no. 1971, pp. 903–995, 1998.

[55] D. P. Mandic, N. U. Rehman, Z. H. Wu, and N. E. Huang, "Empirical mode decomposition-based time–frequency analysis of multivariate signals: the power of adaptive data analysis," *IEEE Signal Processing Magazine*, vol. 30, no. 6, pp. 74–86, 2013.